Supporting Information for: Extended dynamically weighted CASPT2: the best of two worlds

Stefano Battaglia* and Roland Lindh*

Department of Chemistry - BMC, Uppsala University, P.O. Box 576, SE-75123 Uppsala, Sweden

E-mail: stefano.battaglia@kemi.uu.se; roland.lindh@kemi.uu.se

1 Excited States of Glycine

In order to investigate the dependence of vertical electronic excitation energies on the number of model states included in the perturbative calculation, we study the $n_N \rightarrow 3s$ and the $n_O \rightarrow \pi^*$ transitions in the glycine molecule. The former is the transition to the first excited state of the totally symmetric irreducible representation (irrep) within the C_s molecular point group, $2^1A'$, while the latter is the excitation to the $1^1A''$ state. The glycine molecule has a very dense set of excited states below 10 eV of both valence and Rydberg type[1] and it is thus a suitable model to probe the effect of including various numbers of states of different character in the model space.

The computational details are as follows. The geometry was optimized at closed-shell MP2/cc-pVTZ level of theory[2,3] within the C_s point group. This calculation was performed using the Gaussian program package, revision d01.[4] Then, state-average CASSCF calculations were performed for the two symmetry irreps. The active space was composed by 8 electrons in 5 a′ and 4 a″ molecular orbitals. The former were the n_N and n_O lone pairs, the 3s, $3p_x$ and $3p_y$ Rydberg orbitals, while the latter were the three bonding, non-bonding and anti-bonding π orbitals delocalized over the carboxylic acid group and the Rydberg $3p_z$ molecular orbital. The basis set used was the aug-cc-pVTZ one.[5] Two separate calculations were carried out, one averaging over 11 $^1A'$ states, while the other one over 7 $^1A''$ states. Including this number of states was necessary in order to target n$\rightarrow \pi^*$, $\pi \rightarrow \pi^*$ and transitions to Rydberg states from both n and π orbitals. Using these wave functions, MS-CASPT2 and XMS-CASPT2 calculations were carried out, including different number of states in the model space starting with 3 states for the $^1A'$ symmetry sector and 1 state for the $^1A''$ one. To evaluate the excitation energy of $^1A''$ states, the ground state energy was computed by a state-specific CASPT2 calculation using only the lowest CASSCF state (out of the 11 ones available). In the case of MS-CASPT2, calculations were carried out using the canonical method, as well as with a unique state-average Fock operator used for all states, in an analogous manner to the work by Kats and Werner[6]. We shall label results obtained

with the state-average Fock operator as SA-CASPT2. Note that the use of a state-average Fock operator is completely analogous to XMS-CASPT2, the only difference between the methods being the use of rotated states in the latter one. All calculations were performed without the use of the IPEA shift, but including a 0.2 E_h real denominator shift in order to avoid intruder state problems. These calculations were performed using a development branch of OpenMolcas,[7] version 19.11-88-g4984c848.

The vertical transition energies as a function of model space dimension are reported in Figures 1 and 2 for the $^1\mathrm{A}'$ and the $^1\mathrm{A}''$ states, respectively. Canonical MS-CASPT2 shows the weakest dependence on the model space dimension. The estimated excitation energy is consistently the same irrespective of the number of reference states, and only for the largest dimensions they change slightly. On the other hand, both XMS-CASPT2 and SA-CASPT2 are strongly affected by the number of states included. Given that the only difference between the two methods is the use of the rotated states in the former and the original CASSCF states in the latter, this result suggests that it is the use of a unique state-average Fock operator that makes the energy so strongly dependent on the model space dimension. Furthermore, both MS-CASPT2 and SA-CASPT2 use the same reference functions, their only difference is the Fock operator, supporting the conjecture that the differences observed between MS-CASPT2 and XMS-CASPT2 are due to the state-average Fock operator. Note that MS-CASPT2 might as well show a marked dependence on the model space dimension, in particular when the type of transitions are not easily identifiable (i.e. they have a mixed character) and interact strongly with newly included states. Importantly, there is experimental evidence for the $\mathrm{n_O} \rightarrow \pi^*$ transition which is estimated to be between 5.8 and 6.0 eV,[8] thus meaning that, at least in this case, state-averaging truly decreases the accuracy of the method. On the other hand, the oscillations appearing for the $\mathrm{n_N} \rightarrow 3\mathrm{s}$ transition are within the typical error of (X)MS-CASPT2 and thus less compromising. The $^1\mathrm{A}'$ and $^1\mathrm{A}''$ transitions have been computed at the coupled clusters singles and doubles level of theory as well, being estimated at 5.88 eV and 6.32 eV, respectively.[9] The transitions in the example shown

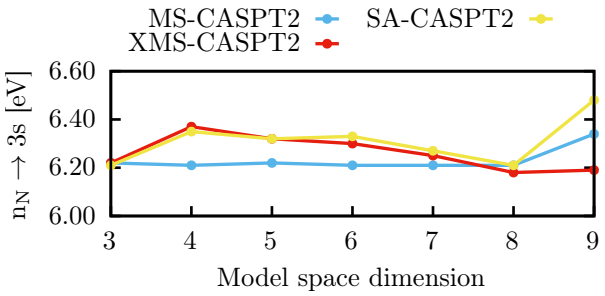

Figure 1: Vertical excitation energy corresponding to the $n_N \rightarrow 3s$ transition as a function of the model space dimension.

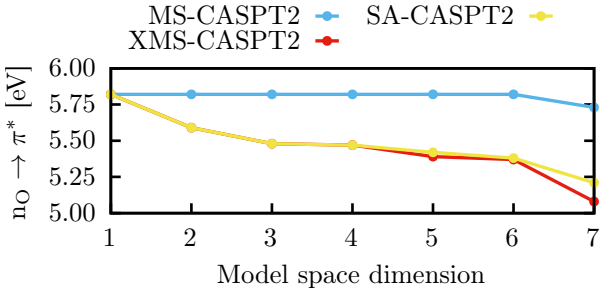

Figure 2: Vertical excitation energy corresponding to the $n_O \rightarrow \pi^*$ transition as a function of the model space dimension.

here were selected because for all methods considered they were clearly identifiable through the transition density matrix and particle/hole transition natural orbitals. This allowed a true comparison between a method using a state-specific Fock operator and methods using a state-average one.

2 Avoided Crossing in LiF

In this section we show additional results for the dissociation of lithium fluoride. First, we report the potential energy curves in the case only two states are included in the calculation. The computational details are the same as reported in the main text, with the only difference being the number of roots considered in both the SA-CASSCF and the various CASPT2 calculations. In Figure 3 we report the results of the reference calculation with MRCISD. The results for XDW-CASPT2 for $\zeta = 50, 5000$ and the limit $\zeta \to \infty$ are shown in Figures 4

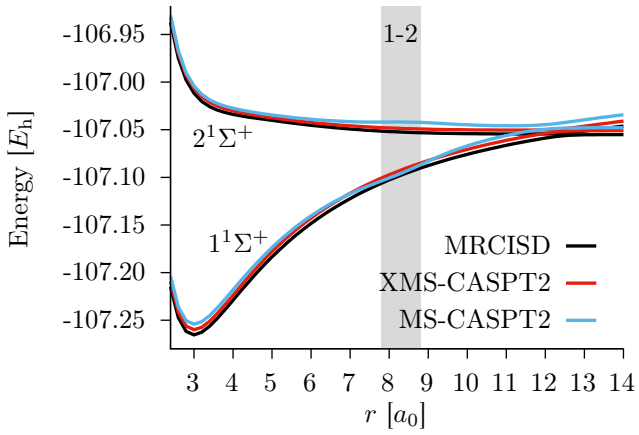

Figure 3: Potential energy curves of the two lowest $^1\Sigma^+$ states of lithium fluoride. The zones highlighted in gray correspond to the avoided crossing regions at the CASSCF level of theory.

to 6.

In the following, we show additional results obtained in the three-state calculations. First, we show in Figure 7 the failure of MRCISD+Q to produce satisfactory potential energy curves. Note that at the position of the second AC, the Davidson's correction leads to an artificial double crossing of the lowest two states. The off-diagonal elements of the Fock operator for $\zeta \to \infty$ in the three-state case (see main text), are reported in Figure 8. Note that the order of magnitude is the same as the other XDW-CASPT2 calculations presented in the main text. The PECs for $\zeta = 500$ are presented in Figure 9 and Figure 10 for calculation with 3 and 2 states, respectively. Density weights and off-diagonal Fock elements are shown

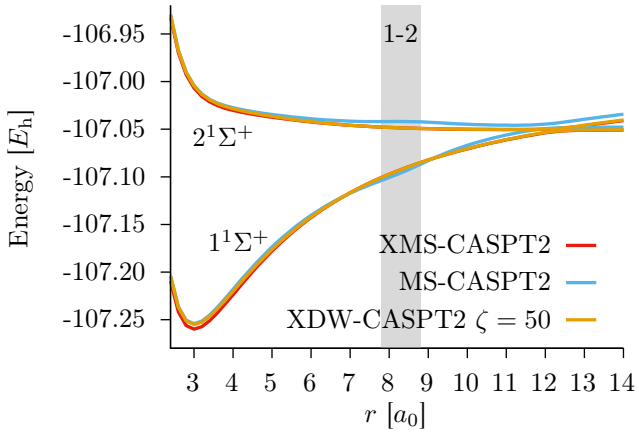

Figure 4: Potential energy curves of the two lowest $^1\Sigma^+$ states of lithium fluoride. Note that to a large extent the XMS-CASPT2 curves are covered by the XDW-CASPT2 ones.

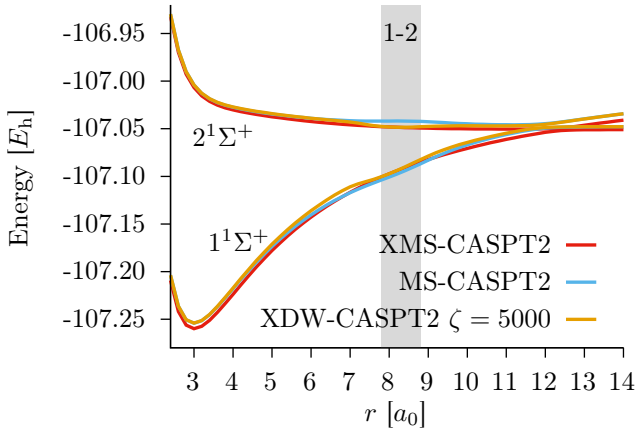

Figure 5: Potential energy curves of the two lowest $^1\Sigma^+$ states of lithium fluoride.

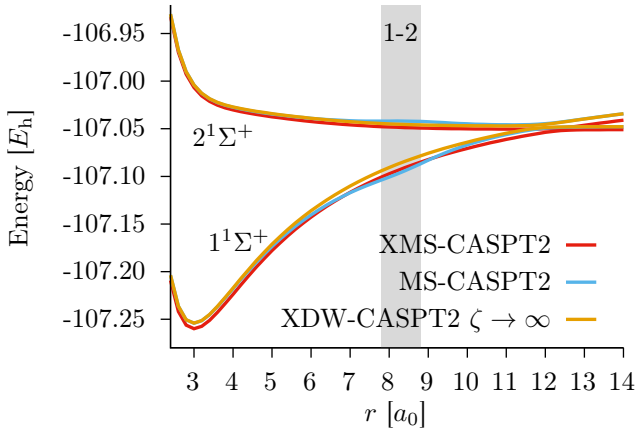

Figure 6: Potential energy curves of the two lowest $^1\Sigma^+$ states of lithium fluoride.

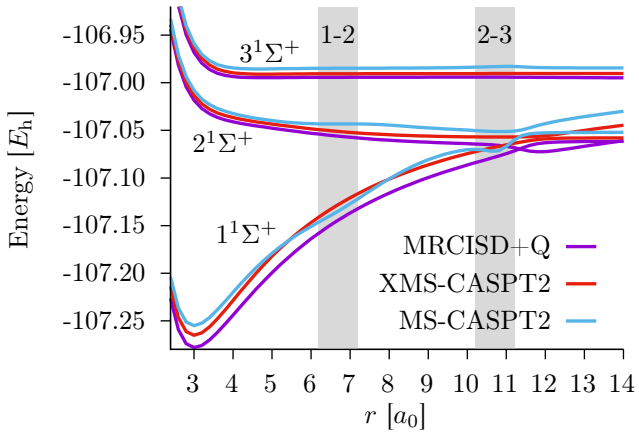

Figure 7: Potential energy curves of the three lowest $^1\Sigma^+$ states of lithium fluoride computed with MRCISD+Q.

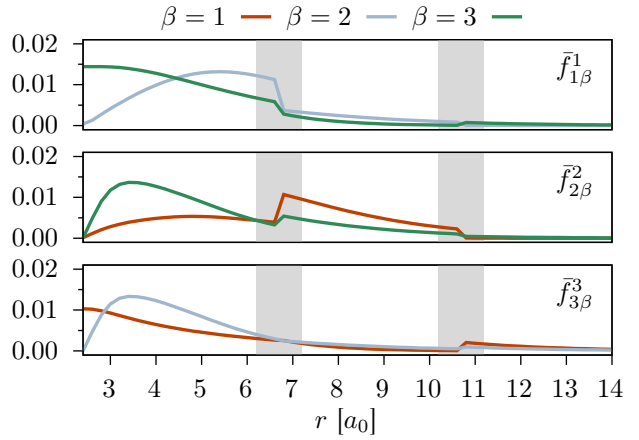

Figure 8: Absolute values of the elements $\bar{f}^{\alpha}_{\alpha\beta}$ for $\zeta \to \infty$. From top to bottom the couplings are for the ground, first excited and second excited state, respectively. Note that for each state (plot), the Fock operator used to compute the couplings is different.

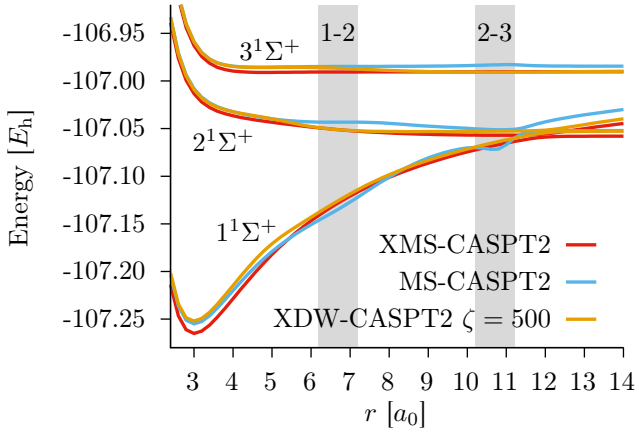

Figure 9: Potential energy curves of the three lowest $^1\Sigma^+$ states of lithium fluoride.

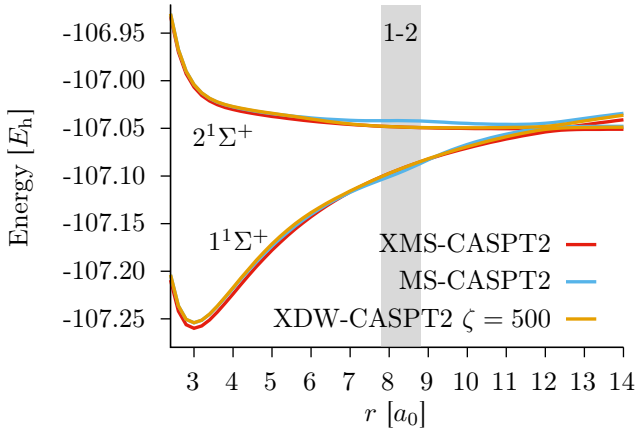

Figure 10: Potential energy curves of the two lowest $^1\Sigma^+$ states of lithium fluoride.

in Figures 11 and 12 for the 3-state calculation with $\zeta = 500$.

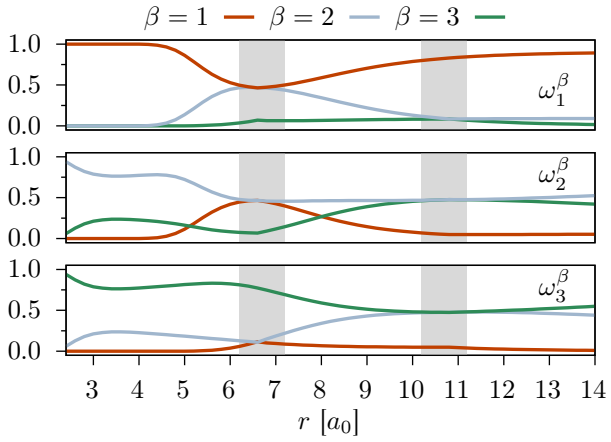

Figure 11: Weights ω_α^β for $\zeta = 500$.

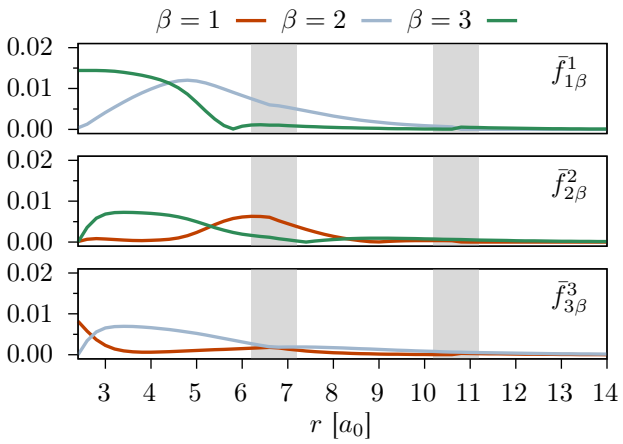

Figure 12: Absolute values of the elements $\bar{f}^{\alpha}_{\alpha\beta}$ for $\zeta = 500$.

3 Conical intersection of allene

In this section we report additional computational details of the calculation involving the distorted allene molecule that complement the description in the main text.

The total number of points in the two-dimensional scan is 6561, 81 for each variable. The scan of the C-C-C-H torsion angle practically corresponds to a pyramidalization of the external carbon atoms. Note that in the original work,[10] the assignment of "variable 1" and "variable 2" in the surface plots were swapped as compared to the explanation in the text.

The IPEA shift was always set to zero for all methods. For some cases it was necessary to include a real denominator shift in order to converge the calculation for all points. In particular the XMS-CASPT2 calculation used a shift of 0.5 Hartree for any size of the model space. The XDW-CASPT2 calculations were thus performed with the same shift in order to compare its results to the XMS-CASPT2 ones, even though a smaller shift was sufficient to avoid intruder states.

In order to have visually comparable results to Ref. 10, we plotted the absolute values of the energy difference between the $1^1A'$ and $2^1A'$ states as a colormap with 64 contour iso-surface lines, using a color palette similar to the one of the original work.

In Figure 13 we report the results for a model space with 6 states for XMS-CASPT2. As discussed in the main text, the PES remains virtually unchanged upon increase of the model space dimension.

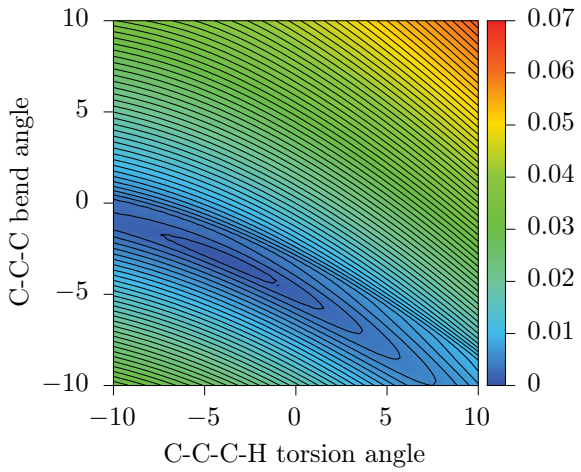

Figure 13: Color-mapped isosurface plot of the absolute energy difference (in E_h) between the $1^1\mathrm{A}'$ and $2^1\mathrm{A}'$ states for a model space including 6 states. The calculation was carried out with XMS-CASPT2.

4 Vertical excitation energies

In this section we report additional information regarding the computational details for the calculation of vertical excitation energies. Imposed molecular point group symmetry, number of active electrons, occupied and active orbitals and real denominator shifts are listed in Table 1. Note that if a shift was necessary for a method, it was also applied to the other ones in order to obtain comparable results.

Table 1: Computational details of CASSCF and CASPT2 calculations. The string of numbers in the occupied and active orbitals follows the irrep convention of OpenMolcas.

Molecule	PG	N_{el}	Occ. MOs	Active MOs	Shift
acetamide	C_s	6	12 1	1 3	0.1
acetone	C_{2v}	6	7 4 1 1	2 1 0 2	0.0
adenine	C_s	12	29 0	0 10	0.1
benzene	C_s	6	18 0	0 6	0.0
benzoquinone	D_{2h}	12	8 0 0 3 0 4 7 0	0 3 1 1 1 1 0 3	0.1
butadiene	C_{2h}	4	7 0 0 6	0 2 2 0	0.0
cyclopentadiene	C_{2v}	4	9 1 0 6	0 2 2 0	0.1
cytosine	C_s	10	24 0	0 8	0.0
formaldehyde	C_{2v}	4	5 0 0 1	0 2 0 1	0.0
formamide	C_s	6	9 0	1 3	0.1
furan	C_{2v}	6	9 0 0 6	0 3 2 0	0.0
hexatriene	C_{2h}	6	10 0 0 9	0 3 3 0	0.0
imidazole	C_s	8	14 0	1 5	0.1
naphthalene	D_{2h}	10	9 0 6 0 0 7 0 7	0 2 0 3 2 0 3 0	0.2
norbornadiene	C_{2v}	4	9 6 3 5	1 1 1 1	0.3
octatetraene	C_{2h}	8	13 0 0 12	0 4 4 0	0.0
propanamide	C_s	6	15 2	1 3	0.1
pyrazine	D_{2h}	10	5 0 0 3 0 4 4 0	1 2 1 0 1 0 1 2	0.2
pyridazine	C_{2v}	10	9 7 0 0	1 1 3 3	0.0
pyridine	C_{2v}	6	11 0 0 7	0 4 2 0	0.2
pyrimidine	C_{2v}	10	10 6 0 0	1 1 2 4	0.1
pyrrole	C_{2v}	6	9 0 0 6	0 3 2 0	0.0
tetrazine	D_{2h}	14	5 0 0 2 0 3 4 0	1 2 1 1 1 1 1 2	0.1
thymine	C_s	12	27 0	0 9	0.1
triazine	C_s	12	15 0	3 6	0.0
uracil	C_s	10	24 0	0 8	0.0

References

(1) Serrano-Andrés, L.; Fülscher, M. P. Theoretical Study of the Electronic Spectroscopy of Peptides. 2. Glycine and N -Acetylglycine. *J. Am. Chem. Soc.* **1996**, *118*, 12200–12206.

(2) Møller, C.; Plesset, M. S. Note on an Approximation Treatment for Many-Electron Systems. *Phys. Rev.* **1934**, *46*, 618–622.

(3) Dunning Jr., T. H. Gaussian basis sets for use in correlated molecular calculations. I. The atoms boron through neon and hydrogen. *J. Chem. Phys.* **1989**, *90*, 1007–1023.

(4) Frisch, M. J.; Trucks, G. W.; Schlegel, H. B.; Scuseria, G. E.; Robb, M. A.; Cheeseman, J. R.; Scalmani, G.; Barone, V.; Mennucci, B.; Petersson, G. A.; Nakatsuji, H.; Caricato, M.; Li, X.; Hratchian, H. P.; Izmaylov, A. F.; Bloino, J.; Zheng, G.; Sonnenberg, J. L.; Hada, M.; Ehara, M.; Toyota, K.; Fukuda, R.; Hasegawa, J.; Ishida, M.; Nakajima, T.; Honda, Y.; Kitao, O.; Nakai, H.; Vreven, T.; Montgomery Jr., J. A.; Peralta, J. E.; Ogliaro, F.; Bearpark, M.; Heyd, J. J.; Brothers, E.; Kudin, K. N.; Staroverov, V. N.; Kobayashi, R.; Normand, J.; Raghavachari, K.; Rendell, A.; Burant, J. C.; Iyengar, S. S.; Tomasi, J.; Cossi, M.; Rega, N.; Millam, J. M.; Klene, M.; Knox, J. E.; Cross, J. B.; Bakken, V.; Adamo, C.; Jaramillo, J.; Gomperts, R.; Stratmann, R. E.; Yazyev, O.; Austin, A. J.; Cammi, R.; Pomelli, C.; Ochterski, J. W.; Martin, R. L.; Morokuma, K.; Zakrzewski, V. G.; Voth, G. A.; Salvador, P.; Dannenberg, J. J.; Dapprich, S.; Daniels, A. D.; Farkas, Ö.; Foresman, J. B.; Ortiz, J. V.; Cioslowski, J.; Fox, D. J. Gaussian 09 Revision D.01. `http://www.gaussian.com`.

(5) Kendall, R. A.; Dunning Jr., T. H.; Harrison, R. J. Electron affinities of the first-row atoms revisited. Systematic basis sets and wave functions and wave functions. *J. Chem. Phys.* **1992**, *96*, 6796–6806.

(6) Kats, D.; Werner, H.-J. Multi-state local complete active space second-order pertur-

bation theory using pair natural orbitals (PNO-MS-CASPT2). *J. Chem. Phys.* **2019**, *150*, 214107.

(7) Fdez. Galván, I.; Vacher, M.; Alavi, A.; Angeli, C.; Aquilante, F.; Autschbach, J.; Bao, J. J.; Bokarev, S. I.; Bogdanov, N. A.; Carlson, R. K.; Chibotaru, L. F.; Creutzberg, J.; Dattani, N.; Delcey, M. G.; Dong, S. S.; Dreuw, A.; Freitag, L.; Frutos, L. M.; Gagliardi, L.; Gendron, F.; Giussani, A.; González, L.; Grell, G.; Guo, M.; Hoyer, C. E.; Johansson, M.; Keller, S.; Knecht, S.; Kovačević, G.; Källman, E.; Li Manni, G.; Lundberg, M.; Ma, Y.; Mai, S.; Malhado, J. P.; Malmqvist, P. Å.; Marquetand, P.; Mewes, S. A.; Norell, J.; Olivucci, M.; Oppel, M.; Phung, Q. M.; Pierloot, K.; Plasser, F.; Reiher, M.; Sand, A. M.; Schapiro, I.; Sharma, P.; Stein, C. J.; Sørensen, L. K.; Truhlar, D. G.; Ugandi, M.; Ungur, L.; Valentini, A.; Vancoillie, S.; Veryazov, V.; Weser, O.; Wesołowski, T. A.; Widmark, P.-O.; Wouters, S.; Zech, A.; Zobel, J. P.; Lindh, R. OpenMolcas: From Source Code to Insight. *J. Chem. Theory Comput.* **2019**, *15*, 5925–5964.

(8) Clark, L. B. Polarization Assignments in the Vacuum UV Spectra of the Primary Amide, Carboxyl, and Peptide Groups. *J. Am. Chem. Soc.* **1995**, *117*, 7974–7986.

(9) Osted, A.; Kongsted, J.; Christiansen, O. Theoretical Study of the Electronic Gas-Phase Spectrum of Glycine, Alanine, and Related Amines and Carboxylic Acids. *J. Phys. Chem. A* **2005**, *109*, 1430–1440.

(10) Granovsky, A. A. Extended multi-configuration quasi-degenerate perturbation theory: The new approach to multi-state multi-reference perturbation theory. *J. Chem. Phys.* **2011**, *134*, 214113.